ELSEVIER

Contents lists available at ScienceDirect

Journal of Magnetic Resonance

journal homepage: www.elsevier.com/locate/jmr



Computer-generated pulse sequences for $^1H^{-15}N$ and $^1H_{\alpha}^{-13}C_{\alpha}$ separated local-field experiments



Joel Lapin, Alexander A. Nevzorov

Department of Chemistry, North Carolina State University, 2620 Yarbrough Drive, Raleigh, NC 27695-8204, USA

ARTICLE INFO

Article history: Received 17 June 2020 Revised 11 July 2020 Accepted 13 July 2020 Available online 17 July 2020

Keywords:
NMR pulse sequence design
Automation
Simulated annealing
GPU computing
Separated local field experiments
Dipolar couplings
PISEMA
SAMPI4
ROULETTE

ABSTRACT

High-resolution separated local field (SLF) experiments are employed in oriented-sample solid state NMR to measure angular-dependent heteronuclear dipolar couplings for structure determination. While traditionally these experiments have been designed analytically by determining cycles of pulses with specific phases and durations to achieve cancellation of the homonuclear dipolar terms in the average Hamiltonian, recent work has introduced a computational approach to optimizing linewidths of the ¹H-¹⁵N dipolar resonances. Accelerated by GPU processors, a computer algorithm searches for the optimal parameters by simulating numerous ¹H-¹⁵N NMR spectra. This approach, termed ROULETTE, showed promising results by developing a new pulse sequence (ROULETTE-1.0) exhibiting 18% sharper mean linewidths than SAMPI4 for an N-acetyl Leucine (NAL) crystal. Herein, we expand on this previous work to improve the performance of the ${}^{1}H^{-15}N$ SLF experiment and extend the work beyond the original approach to new SLF experiments. The new algorithm, in addition to finding pulse durations and phases, now searches for the optimal on/off application scheme of radio frequency irradiation on each channel. This constitutes true de novo optimization, effectively optimizing every aspect of a pulse sequence instead of just phases and durations. With an improved ROULETTE algorithm, we have found a new ¹H-¹⁵N pulse sequence, termed ROULETTE-2.0, yielding 32% sharper mean linewidths than SAMPI4 for NAL crystal at 500 MHz ¹H frequency. Whereas both SAMPI4 and ROULETTE-1.0 have a window where the rf power on the I-channel is turned off, the new pulse sequence is entirely windowless. Furthermore, the reliability of the algorithm has been greatly improved in terms of avoiding false positives, i.e. well-performing pulse sequences in silica that fail to render narrow resonances in experiment. The program has been extended to the ${}^{13}C_{\alpha}{}^{-1}H_{\alpha}$ SLF experiments, using a 6 subdwell architecture similar to the $^1\text{H}-^{15}\text{N}$ optimization. Compared to the PISEMA pulse sequence, the mean $^{13}\text{C}_{\alpha}-^{14}\text{H}_{\alpha}$ linewidth is 17% sharper for the new pulse sequence, termed ROULETTE-CAHA. In addition to superior performance, the work demonstrates the broad applicability of the algorithm and its adaptability to different NMR experiments and spin systems.

© 2020 Elsevier Inc. All rights reserved.

1. Introduction

Structure determination of uniaxially aligned membrane proteins [1–9] and liquid-crystalline materials [10,11] by solid-state NMR is based on the measurement of multiple heteronuclear dipolar couplings (DC's). Recent work has demonstrated that spectral measurements of $^1\mathrm{H}^{-15}\mathrm{N}$ and $^{13}\mathrm{C}_{\alpha}^{-1}\mathrm{H}_{\alpha}$ DCs, complemented with $^{15}\mathrm{N}$ chemical shift anisotropy (CSA), can yield low RMSD backbone folds in oriented protein samples [12,13]. The promise of this method for structure determination depends on the ability to obtain high-resolution NMR spectra that permit unambiguous assignments and subsequent structure calculations. High-

resolution separated local field (SLF) experiments have long been utilized in oriented sample NMR [14–16]. These experiments typically consist of a series of short rf pulses (<20 µs) on both the low/dilute and high/abundant spins, e.g. ¹⁵N and ¹H nuclei. The main goal of the pulses is to cancel all homonuclear interactions in the time-average Hamiltonian, allowing for the measurement of just the heteronuclear couplings. Traditionally the above problem was treated analytically by using the average Hamiltonian theory (AHT), but this method becomes increasingly difficult while attempting to design better-performing pulse sequences involving larger numbers of pulses (subdwells) and non-quadrature phases.

Computer modeling has long proved useful for simulating NMR spectra [17–19] and producing new NMR pulse sequences [20]. A recently proposed method determines pulse sequences (PS) in a

fully automated fashion [21]. This method, termed ROULETTE (Random Optimization Using the Liouville Equation Tailored to the Experiment), is based on optimizing a scoring function for the calculated spectra using a Monte Carlo simulated annealing (MCSA) protocol. In optimizing the scoring function, ROULETTE determines the optimal pulse phases and durations that selectively evolve the desired DCs while yielding the narrowest possible linewidths. The calculation can in principle include numerous pulses or sub-dwells, non-quadrature phases, and a discrete application of rf irradiation. Exhaustive MCSA sampling ultimately allows for the determination of optimal PS parameters, i.e. pulse phases, durations, and an rf irradiation scheme. Moreover, such a strategy does not rely on AHT, but considers realistic many-spin densitymatrix simulations in order to predict PSs capable of yielding best experimental outcomes. Ultimately ROULETTE produced over a dozen of new PS's with superior linewidths to the SAMPI4 PS when run on an NAL crystal. The best of these PS's can be easily refined to further improve the score, or to adapt the parameters to different rf field amplitudes. ROULETTE is also applicable to lossy biological samples, which was previously demonstrated for selectively Leucine-labeled Pf1 coat protein [21].

In spite of the demonstrated performance of ROULETTE, the results have also showed that false positive sequences, i.e. sequences having sharp linewidths in silica but failing experimentally, were also rather common. Therefore, the generated pulse sequences should be screened experimentally in order to find a reliable PS that can be used for structure determination. While for single-crystals such as NAL this can be achieved by running short experiments, the screening of PSs may not be feasible for biological samples, which naturally take longer times to run (by orders of magnitude). Furthermore, previous work was applied only to a single type of SLF experiment, i.e. for ¹H-¹⁵N DC's. It would be of interest to apply this strategy of PS optimization to other types of NMR experiments. Naturally, optimizing for different NMR observables necessitates alterations to the simulated spin system, interaction parameters, and model Hamiltonians.

The present work is aimed at accomplishing the following goals: (1) improving on the optimization $^1\text{H}-^{15}\text{N}$ DCs, (2) increasing the reliability of NMR experiment simulations to predict experimental results, and (3) generalizing this method to computer optimizations of other NMR experiments, namely for $^{13}\text{C}_{\alpha}-^{1}\text{H}_{\alpha}$ DC's. Specifically, we present updates to the fit function, which selects far more reliable and superior PSs when run experimentally. This has allowed us to generate a new PS that provides an even greater improvement over the SAMPI4 sequence. Furthermore, the approach was extended to design a novel sequence for measuring $^{13}\text{C}_{\alpha}-^{1}\text{H}_{\alpha}$ DCs, which improves upon the PISEMA sequence. Taken together, the results demonstrate generality of the ROULETTE approach to optimizing various types of NMR experiments.

2. Methods

2.1. Software and hardware

All calculations were carried out on an Alienware Aurora RB desktop computer with an Intel® Core™ I7-9700 K processor operating at 3.60 GHz. The computer was custom equipped with two NVIDIA GeForce GTX 1080 Ti GPUs, on which the spectral simulations were carried out. A Python simulation code was written specifically to optimally distribute computations over two GPUs.

The code (provided upon request to the authors) has been developed so that administering the main program is done by external input scripts. The most important simulation parameters such as spin coordinates, and experiment specifications are input via text files, which are then read in by the program. The motiva-

tion for this setup was to make the program user-accessible regardless of proficiency in the Python programming language. The code was run primarily in the Anaconda © data science platform, but can be implemented from any appropriate Python supported platform (Unix shell, Jupyter Notebook) as long as all libraries and dependencies are met.

3. Spin system

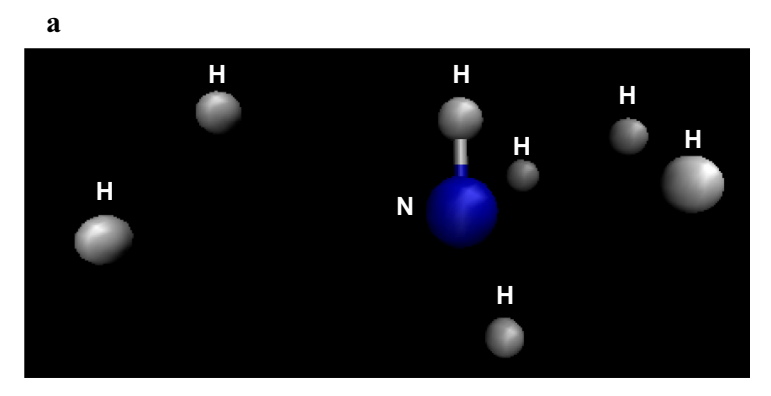
Since the density matrix scales exponentially with the number of spins, generally only fewer than a dozen of spins is practical in terms of the simulation time and memory constraints. The selection of the spins is critical to retaining accuracy. Generally the closest spins to the coupling of interest will have the greatest effect on the system and thus should be included up to a certain cutoff distance. The same coordinates were used for the $^{1}H^{-15}N$ system as in the previous work [22]. The coordinates are generated from a polyalanine alpha helix, and include the seven closest ^{1}H spins to a backbone ^{15}N (all within 3 Å), yielding 8 spins total (cf. Fig. 1a). The coordinates used for simulating $^{13}C_{\alpha}^{-1}H_{\alpha}$ experiments include the three closest ^{13}C atoms and five closest ^{1}H atoms (all within 2.5 Å) to the $^{13}C_{\alpha}$ of interest, totaling 9 spins (cf. Fig. 1b).

Whereas ^{15}N is a more dilute spin, the $^{13}C_{\alpha}$ spin is interacting with other carbons in uniformly labeled samples, and thus $^{13}C^{-13}C$ DC's will need to be canceled out simultaneously with the $^{1}H^{-1}H$ homonuclear interactions, which represents an additional challenge for PS design. Naturally with an additional spin, $^{13}C_{\alpha}^{-1}H_{\alpha}$ optimizations took longer to run than the 8 spin $^{14}H^{-15}N$ system (density matrix dimension of 512 vs 256, respectively).

Another improvement over the previous simulation method was to implement a more accurate method for generating the desired dipolar couplings. In the previous work the value of the coupling for the DC of interest was manually changed prior to calculating the Hamiltonian. Instead of directly setting the desired coupling value, the entire spin system is now rotated until the coupling value is as close to the intended frequency as possible. The implementation uses a simplex solver to find an axis orientation and rotation angle about that axis from 0 to 180°. All DC's change as the bonds in the system rotate, and ultimately the coordinates that yield the closest heteronuclear DC to the intended frequency are used throughout the simulation. For example, if 4 different coupling values are being probed in a simulation, there will be 4 different sets of spin coordinates used to generate their respective Hamiltonians. This contrasts with the previous work in which the coordinates for all spins stayed the same, and only the value of one coupling was changed.

4. The scoring algorithm

The previous ROULETTE algorithm defined a scoring function that was solely focused on optimizing two main aspects; (1) measurement of the relative frequency positions of peaks, prior to the application of a scaling factor, that should appear in the correct ratios given their desired target couplings, and (2) optimization of the collective amplitudes for the probed couplings. The first criterion remains paramount for predicting PSs that successfully decouple homonuclear and heteronuclear interactions. The second goal is to optimize peak sharpness, i.e. the full width of an NMR resonance at a specified peak height (usually at half height). However, directly using the peak width as an objective measure suffers from ambiguity in the absolute position of the peak itself (since the scaling factor for a PS is not known a priori); thus, peak intensity was chosen as a suitable proxy for peak width in the initial concept of the ROULETTE algorithm. Indeed, a well performing PS should yield narrow line widths and, thus, high amplitudes. However,



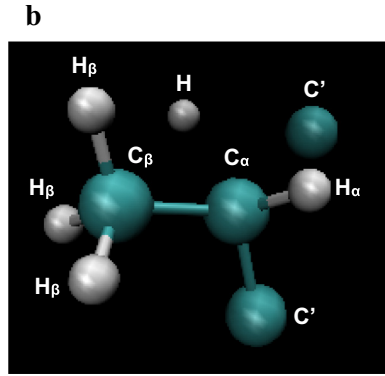


Fig. 1. a) Spin system used for NH optimizations; b) Spin system used for $^{13}C_{\alpha}^{-1}H_{\alpha}$ optimizations, both taken from the coordinates of a polyalanine helix. In a), the spins included are all H atoms that are within 3 Å of the ^{15}N for the $^{14}H_{\alpha}^{-15}N$ of interest, and in b) all C and H atoms are located within 2.5 Å of the $^{13}C_{\alpha}^{-1}H_{\alpha}$ DC of interest.

while intuitively one would expect the peak amplitudes to increase with the narrowing of the peaks, in practice arbitrary dwell times belonging to different PSs can cause these two attributes to become more independent from each other. This is due to the fact that the absolute amplitudes of Fourier-transformed time-domain signals depend on the interval between two successive samples. Therefore, the frequency-domain spectrum needs to be multiplied by the apparent dwell time for a fair comparison of intensities between different PS's. For instance, optimization of unnormalized intensity (as given from direct application of fft transform) could favor abnormally low scaling factors (<0.5) over scaling factors that are closer to those seen in SAMPI4 or PISEMA (0.6-0.8). Taking these considerations into account, the fit function was modified to directly incorporate the in silica measurement of peak widths together with peak intensities. It is important to note, however, that prior to the application of a scaling factor, the frequency scale is arbitrary, and thus the measured linewidths w^{calc} between two different spectra are not directly comparable. Determination of the average scaling factor requires a linear regression for several dipolar couplings, and in the interest of computational efficiency it is preferable to postpone its evaluation until the optimization is finished. Therefore, the peak width is approximated by the ratio of the expected and calculated frequencies for each peak, namely:

$$W_i = W_i^{calc} \begin{pmatrix} f_i^{exp} \\ f_i^{calc} \end{pmatrix} \tag{1}$$

Due to small variability in the scaling factor, this approximation tended to slightly overestimate peak widths for the highest couplings, and likewise produced underestimates for the lowest couplings. In spite of this imperfection, such an approximation was found to be sufficient given the performance of predicted PSs in experiment. Similarly to the previous work, n dipolar couplings having various peak intensities and widths have been first consolidated into their respective geometric means, viz:

$$\langle height \rangle = \left(\prod_{i=1}^{n} I_{i}\right)^{\frac{1}{n}}$$
 (2)

$$\langle width \rangle = \left(\prod_{i}^{n} w_{i}\right)^{\frac{1}{n}} \tag{3}$$

where I_i and w_i are the peak amplitudes (intensities) and widths, respectively, for the generated peak i. The geometric mean ensures that all simulations produce a collectively good result by avoiding a situation where the score could be biased toward one dipolar coupling at the expense of others. In addition, the ratio of the measured couplings between different simulations should be consistent with

the ratio of the true couplings measured between the S and I spins (which in turn depend on the rotated atomic coordinates). This is most easily accomplished by comparing the calculated ratio of frequencies for a pair of peaks with their expected ratio. Ultimately, this work makes two major updates to the scoring function [21], namely: (1) concomitantly optimizing for peak widths and amplitudes; (2) while the previous work used the absolute difference between the expected and calculated frequency ratios, the present work now utilizes a Gaussian shaped function to penalize for this difference. The choice for using a Gaussian function was motivated by its smoother shape, which should facilitate the searching of parameter space as opposed to just taking absolute values [21]. The final form of the fit score function (or pseudoenergy, *E*) used in the present work is given by:

$$E = (wt_w \langle width \rangle - wt_h \langle height \rangle)$$

$$\times \left\{ \prod_{i=1}^{n-1} \left[\Omega - (\Omega - 1) \exp\left(-\left(\frac{f_{i+1}^{calc} / f_i^{calc} - f_{i+1}^{exp} / f_i^{exp}}{z} \right)^2 \right) \right] \right\}^{\frac{1}{n-1}}$$

$$\tag{4}$$

The exponential function in the second term of (Eq. (4)) evaluates the difference between the frequency ratios of the calculated couplings between two successive simulations f_{i+1}/f_i and the ratios of the true (or expected) couplings. In (Eq. (4)), the deviation parameter z ultimately determines precision for the expected frequency ratios between successive simulations. The parameter Ω sets the maximum penalty for incorrectly evolved DC's. In this work, Ω was tuned to effectively penalize violations of peak ratios, and largely depended on the PS architecture. In practice the Ω values ranged from 3 to 100. An increase of Ω had to be complemented with a congruous increase of z, which in turn ranged from 0.4 to 10 to maintain an appropriate shape near the nadir of the function. The nature of the quantities (width) and (height) necessitates additional consideration of their respective weighting factors, wt_w and wt_h . These weights need to be determined for the spin system of interest in order to tune the relative contributions of $\langle width \rangle$ and $\langle height \rangle$ to the fit function. To keep (Eq. (4)) positive, the inequality $wt_w \langle width \rangle > wt_h \langle height \rangle$ must hold. This condition is ultimately upheld by an appropriate choice for wt_h . The peak intensity should generally increase in magnitude as the spectrum gets sharper. In the original ROULETTE, optimizing peak intensity meant that the objective function was minimized to the most negative (<0) quantity possible. By contrast, (Eq. (4)) is a positive quantity decreasing in magnitude as the spectrum gets sharper. This changed the original problem from being a minimization to the most negative value, to a minimization to the least positive value possible. The determination of appropriate values for wt_w and wt_h was based on the relative magnitudes of $\langle width \rangle$ and

 $\langle height \rangle$, to ensure that the quantities were jointly optimized. The minus sign in (Eq. (4)) conceptually renders $\langle height \rangle$ as a "discount" to $\langle width \rangle$. Thus, $\langle width \rangle$ is intended to primarily drive the optimization. To maintain the scoring function as a positive quantity, the upper bound of wt_h must satisfy the following condition:

$$wt_h^{upper} \le \frac{wt_w \langle width \rangle_{min}}{\langle height \rangle_{max}} \tag{5}$$

In this work the weight for peak width, wt_w , was always set to 1. Naturally, in fully optimized sequences, $\langle width \rangle$ will reach its minimum and $\langle height \rangle$ its maximum. Due to the different interaction parameters, coordinates, and spin systems, these respective values were different between $^1H^{-15}N$ and $^{13}C_{\alpha}^{-1}H_{\alpha}$ simulations. After the additional multiplication of the total dwell by a factor of 10^4 , the maximum $\langle height \rangle$ was around 15 for the generated $^1H^{-15}N$ sequences while the minimum $\langle width \rangle$ was typically between 200 and 300 (Hz). For $^{13}C_{\alpha}^{-1}H_{\alpha}$ sequences the maximum $\langle height \rangle$ varied between 3 and 5 and the minimum $\langle width \rangle$ was between 400 and 500. The wt_h values ultimately chosen for optimizing the two experiments were 15 and 100, respectively.

The Python function tasked with identifying and quantifying the peaks in a 1D spectrum is find peaks from the scipy.signal library. A direct approach to this problem would be to measure all peaks in the spectrum without any conditions. This risks considering small artifacts in a spectrum which, by virtue of their unsubstantial shape and intensity, would have smaller peak widths than any real, intense peak. Conversely, setting strenuous conditions for defining peaks risks not measuring any, which is uninformative to the algorithm as it seeks to optimize the fit function. A compromise was found between these two extremes by imposing rather loose conditions for what constitutes a peak, and then penalizing for the presence of unsubstantial artifacts. Since artifacts tended to cluster near the middle and edges of the spectra, the program defined a specific range in which to look for the peak, often 1 kHz from both the negative edge and the center of the spectrum. Amongst all identified peaks, only the most prominent was considered since only one heteronuclear DC resonance is expected for the spin system of interest. There were three main quality control measures implemented in the event that an identified peak had an erroneously low linewidth, perhaps because it was a small artifact rather than a true resonance, or had a serrated shape. First, the minimum target peak width was set to 80 Hz for ¹H-¹⁵N DC's, and 150 Hz for ${}^{13}C_{\alpha}$ - ${}^{1}H_{\alpha}$ DC's. These values were determined by trial and error. Second, while peak width is often measured at half height, it was more effective to measure width closer towards the base (for simulation purposes only). In this work measuring the full peak width at a height fraction of 0.85 from the top was sufficient (instead of the more conventional 0.5). Third, in spite of their linewidth, peaks too unsubstantial to be considered as true resonances tend to have low intensity. While the minimum peak intensity threshold can be passed as an argument to the find_peaks function, such an option often led to no identification of any peaks in the spectrum when the algorithm was in a suboptimal parameter space. To account for such a scenario, a penalty for the measured linewidth using a pre-defined intensity threshold is imposed:

$$W_{i}^{corr} = W_{i}^{meas} \left(\frac{I_{thr}}{I_{meas}}\right)^{\epsilon} if \ I_{meas} < I_{thr}$$
 (6)

Here the correction penalty applies only if the measured intensity is less than I_{thr} , which prevents (Eq. (6)) from further affecting the score above the threshold. The parameter ε allows the effect of the ratio to be amplified or attenuated, and was often set to 1.2,

while I_{thr} was always set to 1.0. If I_{thr} is not surpassed then the equation will increase the apparent registered peak width, which is then used in (Eqs. (3) and (4)).

Previous work used a simulated annealing protocol with the Metropolis criterion [23] in order to search and optimize the PS parameter space. Simulated annealing is implemented by lowering the temperature slowly, defined in (Eq. (7)) by an inverse temperature parameter, W, in order to maintain an equilibrium sampling of the Boltzmann distribution of states as the algorithm descends in pseudoenergy, E. Namely, the Metropolis criterion reads:

Accept move if
$$\exp(-W\Delta E) > rand(0-1)$$
 (7)

In general, this process works for a relatively smooth and well-behaved fit function. Equation (4) does not meet this criterion, since small changes in some parameters can radically change the shape of the spectrum, and thus the score. Simply running a simulated annealing protocol, i.e. slowly increasing W throughout the simulation, risks locking the search into high-score traps, and preventing the broad search of parameter space. For the optimization presented in this paper, the temperature schedule was augmented with an adaptive thermostat. Adaptive temperature in this context means either increasing or decreasing the temperature at regular intervals in order to maintain a certain proportion of uphill moves. This allows the algorithm enough flexibility to jump out of high score traps, as well as driving it downhill to the best score possible. The inverse temperature was adjusted according to the previous sampling history by using the following approximation:

$$W_{i} = W_{i-1} \frac{\exp(-\overline{W}_{i-1}\Delta Q)}{p} if \quad E < E_{thr}, else \quad W^{SA}(i)$$
(8)

That is, the current inverse temperature W_i is determined based on whether a score threshold E_{thr} is crossed, above which a linear simulated annealing schedule is used, and below which adaptive temperature is used. The linear schedule W^{SA} for every increment step is predetermined at the beginning of the program. The adaptive temperature protocol utilizes the past history of the pseudoenergy jumps. ΔE . Parameter ΔO is a list of ΔE values for the past anumber of uphill steps. The purpose of ΔQ is to give a sense of the score landscape in the current parameter space, so that the next temperature can be determined to achieve a p proportion of uphill steps. The previous temperature W_{i-1} is then rescaled by the ratio of the average value of the Metropolis criteria implemented for all members of ΔQ , and the desired proportion of uphill steps p. The main idea of (Eq. (8)) is to allow the simulated annealing protocol to broadly search the parameters at high temperature/ low W, and when the score (pseudoenergy) becomes sufficiently low, i.e. a good candidate for a decoupled sequence is found, the algorithm would then sharply pursue the minimum using the adaptive temperature schedule. This combined temperature protocol delivered reliable and consistent results for almost all simulations, which eases the requirement for running numerous trials in anticipation of failed optimizations. For this work q was set to 200, which was sufficient to accurately predict the next temperature. The parameter p was typically chosen as to maintain 5% uphill steps per temperature level. The score threshold E_{thr} was set to 4,000. The linear simulated annealing schedule incremented the inverse temperature from $W = 10^{-5}$ to $W = 5 \times 10^{-3}$.

To ensure the algorithm works for a variety of orientations and DCs, four target splittings were run per evaluation of pseudoenergy, (Eq. (4)). For $^{1}\text{H}-^{15}\text{N}$ sequences, the full dipolar splittings were 5, 10, 15, and 20 kHz; whereas for $^{13}\text{C}_{\alpha}^{-1}\text{H}_{\alpha}$ PS's, which have a DC constant more than twice as large as $^{1}\text{H}-^{15}\text{N}$, the splittings were 10, 20, 30, and 40 kHz. Experimentation with various PS architectures revealed that some schemes are more conducive to optimization than others. The preferred PS architecture for opti-

mization consisted of 6 subdwells (cf. Fig. 2a), which tended to minimize the fit function most effectively, although up to 9 subwells have been considered (results not shown). Mirror antisymmetry was imposed for phases, meaning mirrored subdwell pairs, i.e. first and last, second and fifth, etc, always differed by 180°, i.e. $\phi_{i,i} = \phi_{i,N-i+1}$ (for N subdwells). Imposing such antisymmetry reduces the number of optimization parameters and conforms to many existing pulse schemes that are typically based on canonical matrix transformations involving average Hamiltonians [14–16]. Mirror symmetry (first equal to last, second equal to next to last... etc) was imposed for pulse durations and ω_{rf} amplitudes. Pulse phases naturally ranged from 0 to 360°. Durations were randomized within a range of 0.5-4, in the units of the 90-degree pulse, t_{90} . The rf amplitudes were specified as Boolean variables, i.e. either on or off. The ¹H-¹⁵N simulations (and experiments) had an $\omega_{\rm rf}$ amplitude of 58.14 kHz, while $^{13}{\rm C}_{\alpha}$ - $^{1}{\rm H}_{\alpha}$ PS's were optimized at 63 kHz. Each simulation had 100 temperature increments, with 200 random steps per temperature. The FID in each simulation was sampled at 256 t₁ points. Longer refinements were often needed, especially if the score was still decreasing upon reaching the maximum number of pre-defined iterations.

5. Results

5.1. Simulations

To illustrate the in-silica performance of ¹H-¹⁵N SLF experiments, shown in Fig. 2b is the simulated result for the new top experimental PS, ROULETTE-2.0, which is compared to our previous top sequence, ROULETTE-1.0, and SAMPI4.

One important aspect of Fig. 2b is the retroactive scoring of the previously developed ROULETTE 1.0 and SAMPI4 by (Eq. (4)). Their scores in the low 200's are still rather good considering that neither was optimized with the score fit function used in this work. ROULETTE-2.0 had both the sharpest parameter $\langle width \rangle$ and highest $\langle height \rangle$ (as given by Eqs. (2) and (3)), while ROULETTE-1.0 was previously optimized for the $\langle height \rangle$ alone. It is also clearly evident from the spectra that the individual resonances line up almost exactly with their expected dipolar couplings. We hypothesize that this result is due to an improved optimization by using the new adaptive temperature protocol, which attains global minima more efficiently.

ROULETTE-1.0, having a relatively large scaling factor of 0.589, represents a rather exceptional example for the previous

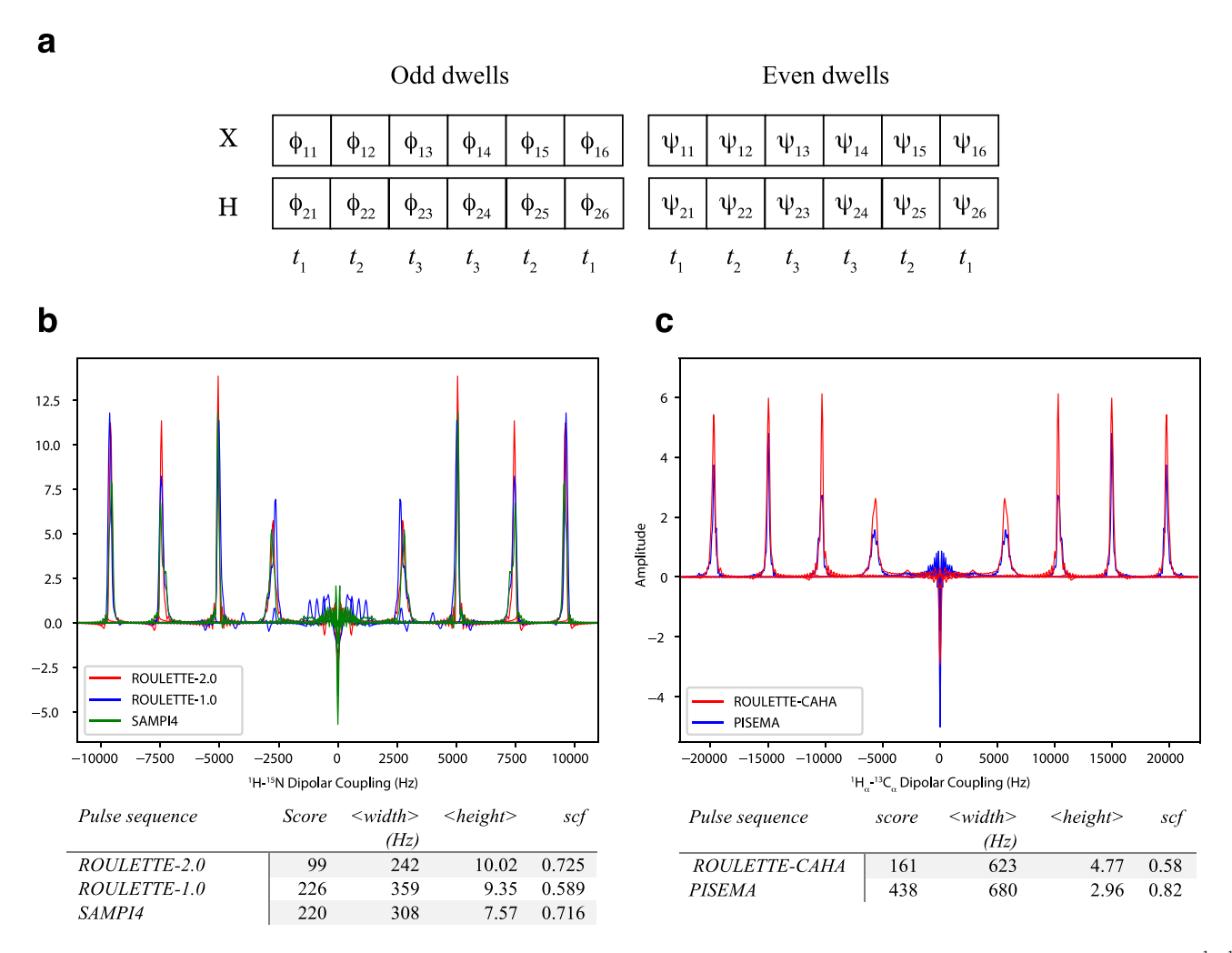


Fig. 2. A. Generic ROULETTE pulse sequence architecture showing six (6) odd and 6 even subdwells. All pulses are applied on resonance. B. The simulation results for $^1H^{-15}N$ ROULETTE-2.0, ROULETTE-1.0, and SAMPI4. For each PS, four (4) simulations were run at the full target dipolar splittings of 20, 15, 10, and 5 kHz. C. The $^{13}C_{\alpha}^{-1}H_{\alpha}$ simulation results for ROULETTE-2.0 as compared to PISEMA. The four target dipolar splittings for the simulations were 40, 30, 20, and 10 kHz. Shown below the spectra are the tabulated results of the PSs, including the unitless average $\langle height \rangle$ (Eq. (2)), $\langle width \rangle$ in Hz, (Eq. (3)), unitless score (Eq. (4)), and the theoretical scaling factor, scf. All spectra are plotted with scf applied to their respective frequency domains.

algorithm. Many of the previous solutions had scaling factors<0.5, well below that of SAMPI4 (0.72). While optimizing *scf* is impractical, the unusually low values of *scf* could be an indicator for false positives. It is also likely that scoring the intensity alone can lead the optimization astray. Almost all optimized sequences under the new method had *scf* between ca. 0.6–0.8. Since these sequences tend to have longer dwells, and thus smaller frequency domains, their scaled peak widths tend to be narrower than for pulse sequences with short dwells. This justifies optimizing the collective line widths together with other spectral attributes.

Since SAMPI4 can only probe maximum DC's of up to ca. \pm 14 kHz at a typical rf amplitude of ca. 60 kHz, $^{13}C_{\alpha}^{-1}H_{\alpha}$ optimizations were compared to PISEMA which is capable of covering the required range of the dipolar couplings (\pm 23 kHz) at this rf field. Fig. 2c displays PISEMA overlayed with the simulation of the best experimentally performing optimization, titled ROULETTE-CAHA. While both sequences exhibit good theoretical widths, ROULETTE-CAHA has a 61% higher $\langle height \rangle$ score. Once again, the comparison shows that the optimization algorithm effectively accomplishes its goal of minimizing the desired fit function.

ROULETTE-2.0 was optimized at $\omega_{\rm rf}$ = 58.14 kHz; ROULETTE-CAHA was optimized at $\omega_{\rm rf}$ = 63 kHz; The phases for the X (i = 1) and H channels (i = 2) corresponding to odd-dwells (ϕ_{ij}) and even dwells (ψ_{ij}) are given for the subdwells j = 1, 2, 3 only, with the phases for j = 4, 5, 6 being mirrored and additionally shifted by 180° (cf. the text). All rf pulses are applied on resonance.

Both pulse sequences have a 6-subdwell architecture to evolve the t_1 dipolar dimension, cf. Table 1. Table 1 also summarizes the relevant pulse parameters for the two new SLF sequences, one optimized for the subsequent ¹H-¹⁵N experiments and the other for ${}^{13}C_{\alpha}$ - ${}^{1}H_{\alpha}$ experiments referred to as ROULETTE-2.0 and ROULETTE-CAHA, respectively (Bruker Topspin 2.0 pulse programs are provided in Supplementary material). These PSs, among others optimized in this work, displayed better linewidths than their respective counterparts, SAMPI4 and PISEMA. Unlike the pulse sequences optimized in the previous work [21], which essentially followed SAMPI4 power application scheme, the present pulse sequences are "windowless", i.e. the rf power on both channels is always on. As a consequence, these sequences have additional phases ϕ_{23} and ψ_{23} , whereas for ROULETTE-1.0 these values were not applicable since the power was off on subdwells 3 and 4 for the I-channel. It is interesting to note that the majority of the simulations indeed converged to rf power being all on, suggesting that this may be an optimal pulse application scheme for SLF experiments. PS's with windows and relatively low scores have also been tested experimentally; however, the resulting linewidths were inferior to those observed in the windowless sequences (results not shown).

6. Experimental results on NAL at 500 MHz ¹H frequency

All NMR experiments were run on a 500 MHz 1 H spectrometer using an NAL single crystal (18 mg). The majority of the generated 1 H- 15 N pulse sequences rendered sharp spectra. The RF amplitudes were experimentally calibrated at $\omega_{\rm rf}$ = 58.14 kHz, for 1 H- 15 N experiments and at $\omega_{\rm rf}$ = 61.4 kHz for 1 H $_{\alpha}$ - 13 C $_{\alpha}$ experiments, i.e.

Parameters for ROULETTE-2.0 and ROULETTE-CAHA pulse sequences.

the same or nearly the same as the ones used in the optimizations. Fig. 3 shows the spectrum of ROULETTE-2.0 overlaid with SAMPI4 for comparison. A marked improvement in the dipolar linewidths over SAMPI4 can be seen for all four peaks in the spectrum.

It should be noted that implementing the newly optimized pulse sequences on a 500 MHz spectrometer having three dedicated rf amplifiers for the three channels (1H, 13C, 15N) has greatly improved the linewidths for the computationally optimized pulse sequence vs. SAMPI4. This suggests that the false positives previously reported for the 300 MHz spectrometer may in fact have been false negatives, i.e. potentially viable PSs that yielded broad resonances in experiment. ROULETTE-2.0 now exhibits 32% sharper average linewidths over SAMPI4 (measured conventionally as full peak widths at half peak heights), as compared to just 18% sharper average linewidths for ROULETTE-1.0, previously obtained on the 300 MHz spectrometer [21]. The latter was equipped with a dual amplifier for both channels, for which slower rise time and more visible pulse distortions have been observed. We also note that the gains are reported here as the percentage difference, i.e. the difference between the two linewidths divided by the average between the two values. Furthermore, whereas there was previously a notable disparity [21] in the frequencies of higher dipolar couplings between the ROULETTE pulse sequences and SAMPI4, now the measured spectra overlap nearly perfectly.

The ¹³C-detected spectrum, acquired using the ROULETTE-CAHA sequence (Table 1), is shown in Fig. 4 for comparison with PISEMA [14]. Similarly to $^{1}\text{H}-^{15}\text{N}$ DC's, the $^{13}\text{C}_{\alpha}-^{1}\text{H}_{\alpha}$ SLF spectrum of NAL contains 4 intense resonances for $^{13}\text{C}_{\alpha}$ carbons, but there are also additional resonances from other ¹³C sites of the molecule, such as carbonyl, beta, gamma, and methyl carbons (up to 32 total). The ${}^{13}C_{\alpha}{}^{-1}H_{\alpha}$ resonances of interest can be readily assigned by the presence or absence of additional 13 C $_{\alpha}$ - 15 N splittings when measured with and without ¹⁵N decoupling. The PISEMA spectrum of Fig. 4a (blue contours) identifies the $C_{\alpha}H_{\alpha}$ peaks ranging from 10 to 20 kHz, as evident by the presence of doublets when compared to the ¹⁵N-decoupled ROULETTE-CAHA (red contours), which exhibits ¹³C₀ NMR resonances in between. The fourth peak, around (32 ppm, 9 kHz), does not completely split for un-decoupled PISEMA, but still can be identified by its broader intensity distribution. Fig. 4b allows for a more direct comparison of linewidths when ¹⁵N decoupling is applied in both experiments. The ROULETTE-CAHA PS has a 17% sharper mean linewidth (also reported here as a percent difference) when compared to the

An important aspect of computer-generated pulse sequences is their robustness and scalability of the subdwell timings with respect to arbitrary rf amplitudes. We have refined ROULETTE-CAHA at a relatively modest rf frequency amplitude of 50 kHz, which resulted in a slight re-optimization of the phases and timings originally obtained at 63 kHz rf amplitude (cf. Table 1). It should be noted that neither PISEMA nor SAMPI4 would be able to properly evolve the largest observable $C_{\alpha}H_{\alpha}$ coupling of ca. 19.5 kHz at this rf amplitude since the corresponding Nyquist frequencies in the dipolar dimension would be smaller than this value. Fig. 5 shows the full ROULETTE-CAHA spectrum exhibiting additional 13 C resonances present in NAL including the carbonyl, beta, gamma, and methyl carbons. The latter can be easily identi-

Sequence	ϕ_{11}	ϕ_{12}	ϕ_{13}	ϕ_{21}	ϕ_{22}	ϕ_{23}	ψ_{11}	ψ_{12}	ψ_{13}	ψ_{21}	ψ_{22}	ψ_{23}	$t_1(\mu s)$	$t_2(\mu s)$	t ₃ (μs)
ROULETTE-2.0	201.5	189.6	141.3	247.5	288.1	181.9	176.4	151.9	272.5	153.8	165.3	72.7	10.99	3.19	6.46
ROULETTE-CAHA	234.7	159.4	257.9	228.1	155.3	197.8	65.1	5.4	287.5	285.5	7.4	185.8	6.48	5.15	2.16

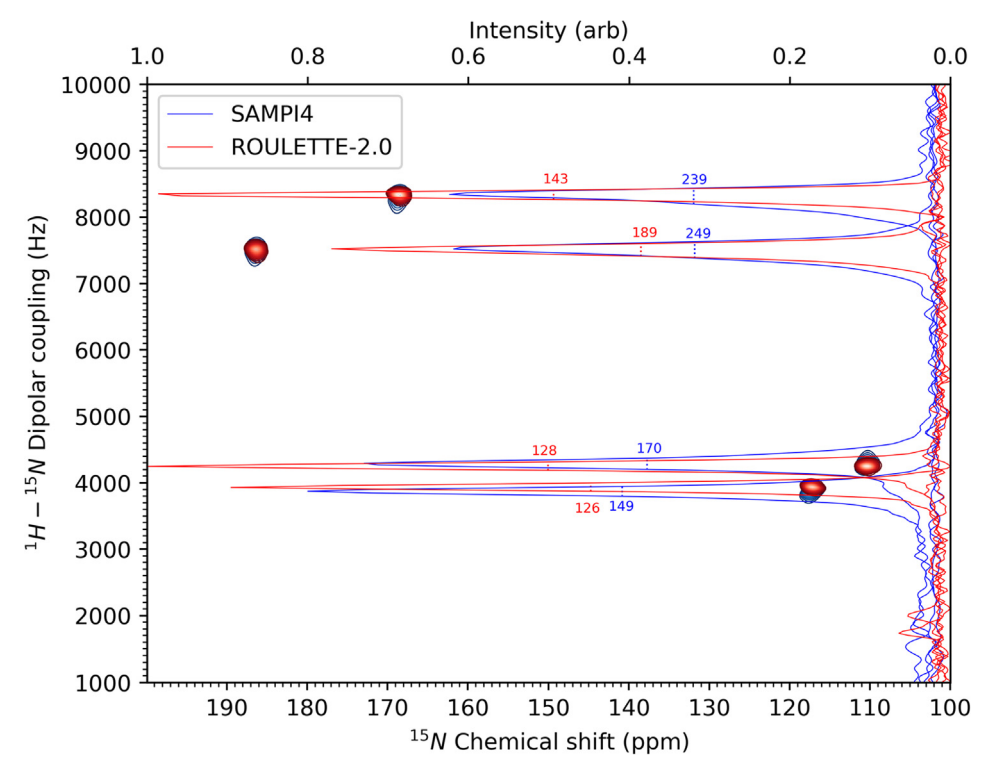


Fig. 3. Overlay of SLF spectra of NAL crystal obtained using pulse sequences SAMPI4 vs. ROULETTE-2.0 (from Table 1) correlating the dipolar ¹H-¹⁵N dimension with ¹⁵N CSA. Individual linewidths in the ¹H-¹⁵N dimension measured at half peak heights are indicated in Hz. The mean linewidth amongst the 4 peaks is 201.75 and 146.5 Hz for SAMPI4 and ROULETTE-2.0, respectively (yielding a 32% average gain in resolution).

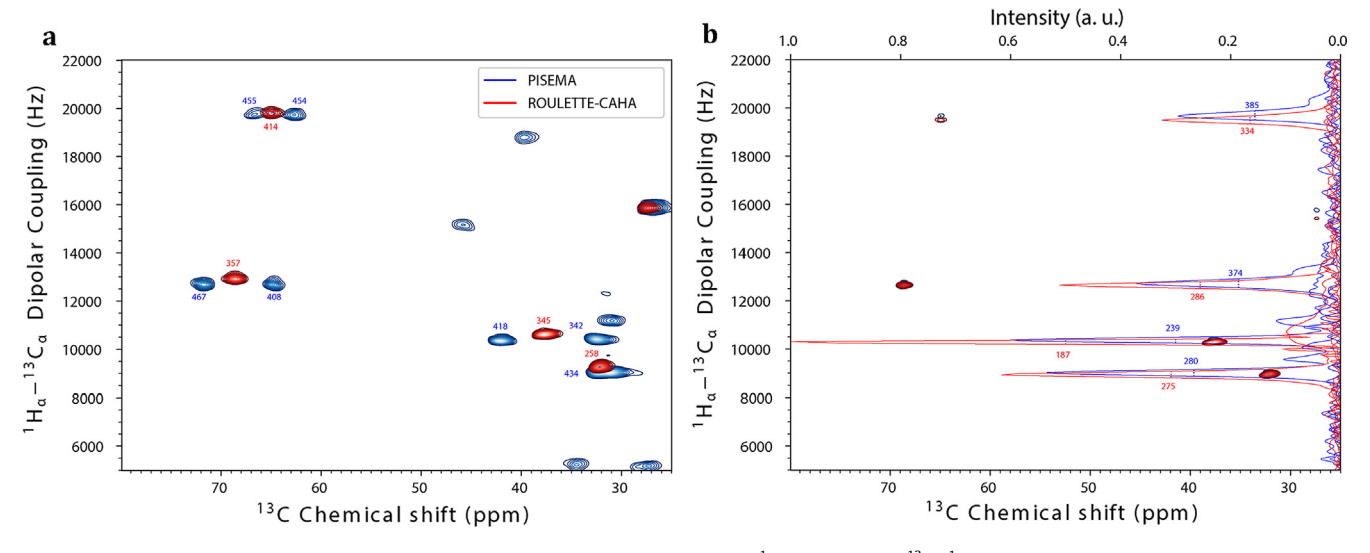


Fig. 4. Overlays of PISEMA and ROULETTE-CAHA (cf. Table 1) spectra of NAL crystal at 500 MHz 1 H frequency. The 13 C $_{\alpha}$ - 1 H $_{\alpha}$ DC dimension, along the y-axis, is correlated with 13 C CSA, along the x-axis. In a), the PISEMA experiment (blue) was run without 15 N decoupling, allowing one to easily identify 13 C $_{\alpha}$ resonances; by contrast, ROULETTE-CAHA (red) was run with 15 N decoupling. In b), both PISEMA and ROULETTE-CAHA, were run with 15 N decoupling. All four relevant resonances are marked with their corresponding linewidths (in Hz) in the DC dimension. The mean linewidths in b) are 319 Hz and 270 Hz for PISEMA and ROULETTE-CAHA, respectively. The unmarked peaks correspond to the aliphatic carbons, presumably arising from 13 C $_{\theta}$ sites.

fied by the dipolar quadruplets produced by CH_3 spin systems in the doubly tilted rotating frame under the spin-lock conditions [24]. As can be seen, all dipolar couplings are evolved at 50 kHz rf field strength with linewidths comparable to those obtained at the higher rf field. We would like to note that well resolved resonances could be obtained even without any optimization by simply rescaling all subdwell timings by the ratio 63/50 while keeping the same phases.

7. Discussion

The original ROULETTE implementation [21] has left several outstanding issues pertaining to the feasibility of the method. The presence of frequent false positives between the simulations and experiment suggested a shortcoming of the optimization method used in the previous version of ROULETTE. Furthermore, despite promising results for ¹H-¹⁵N DC's, only phases and dura-

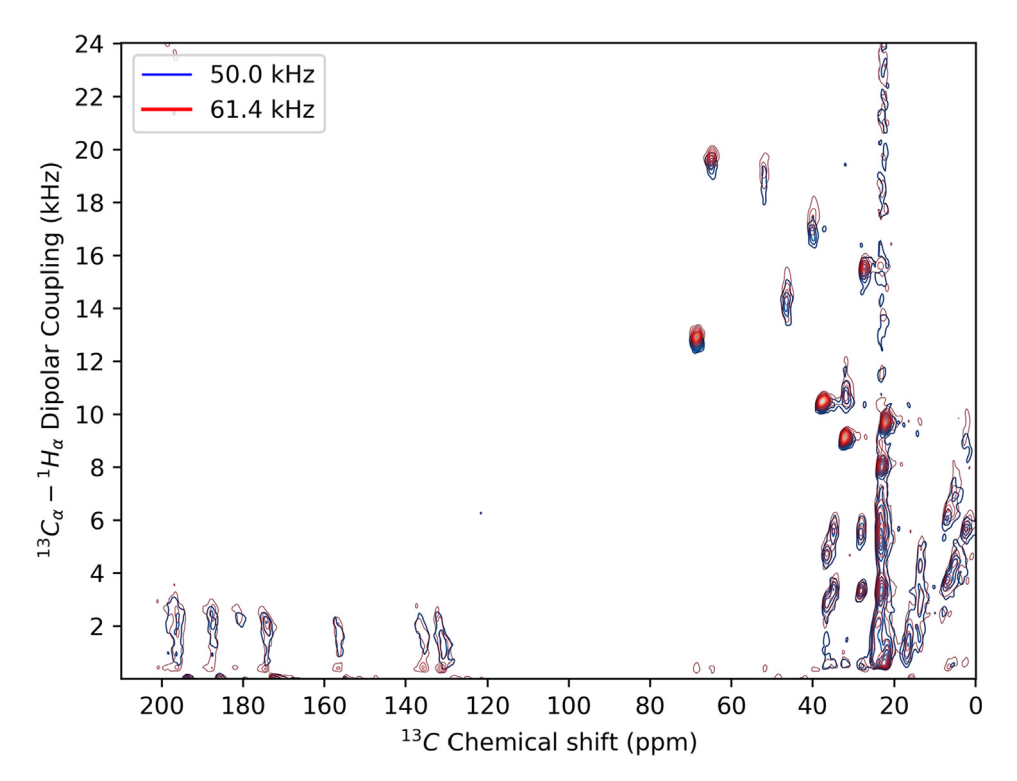


Fig. 5. ROULETTE-CAHA spectrum of NAL crystal, refined at $ω_{rf}$ = 50 kHz (blue contours), overlayed with the spectrum obtained at $ω_{rf}$ = 61.4 kHz. The four most intense 13 C $_{\alpha}$ - 13 H $_{\alpha}$ resonances are located between 9 and 20 kHz and 30–70 ppm in the 13 C chemical shift dimension; many other 13 C resonances are also evolved including the carbonyl (>120 ppm), beta, gamma, and methyl 13 C resonances (at < 40 ppm and < 8 kHz DC's).

tions were optimized while using the existing power application scheme of SAMPI4. The present work has addressed those outstanding questions and improved on the strategy for automated de novo PS design.

Several critical modifications of the algorithm appear to have improved the efficacy of the optimization protocol. It is likely that the adaptive temperature protocol has significantly improved the algorithm's ability to minimize the score, irrespective of the choice for the fit function. Simulated annealing, while effective for smoother energy surfaces, often struggles to find stable minima on complex energy surfaces that have many barriers and local minima. This may be the case in evaluating PSs with many fitting parameters and a complicated fit scoring function, cf. (Eq. (4)). The adaptive temperature protocol strategically increases or decreases the temperature to ensure a reasonable amount of uphill moves so that the parameter space is adequately searched. Furthermore, the program has been developed to easily extend or refine any previously optimized sequence. This expands on the simulation tools at the disposal of the user for pulse sequence simulations and optimizations.

A further important modification was the addition of rf amplitudes as optimization parameters. The first version of ROULETTE only optimized for pulse phases and durations. Adding the rf amplitudes as fitting parameters transforms ROULETTE into a true *de novo* pulse sequence design method. Despite greatly increasing the parameter space for the fit function, the algorithm was able to handle more variables without getting stuck in local minima.

The simulation results also suggest that the new fit scoring function (Eq. (4)) has greatly benefitted the algorithm in selecting viable PSs. With the inclusion of the mean spectral widths to the fit function, now the scaling factors of all optimized sequences fall within a narrow range (0.6-0.8). Previously, using only the mean heights together with the DC frequency ratios generally produced two families of solutions: one with small scfs and one with larger

scf's closer to that of SAMPI4 or PISEMA. The consistency in the scaling factors between different optimizations suggests that the fit function now converges to a consistent pulse sequence architecture, and is less prone to random local optimizations than the previous fit function.

Experimental results on the 500 MHz spectrometer have allayed several concerns that emerged from the previous work with ROULETTE. The false positive outcomes, i.e. well-scoring sequences in the simulation but ineffective in the experiment, have largely been absent on the 500 MHz spectrometer. More importantly, amongst the computationally optimized pulse sequences, there was no longer any pronounced disparity among the experimental frequencies for ¹H-¹⁵N DCs for all 4 peaks of NAL as measured by ROULETTE vs. SAMPI4. Moreover, instead of the previous improvement of 18% for the mean linewidths over SAMPI4, ROULETTE-2.0 has now demonstrated a 32% improvement on the 500 MHz spectrometer. All the above improvements over the earlier results strongly indicate that the previous false positives were in reality false negatives, and that the more basic hardware of the 300 MHz spectrometer was not suitable for properly implementing the complex pulse sequences.

Optimizing pulse sequences for evolving $^{13}\text{C}_{\alpha}^{-1}\text{H}_{\alpha}$ DC's presented new challenges for both the algorithm and the experimental testing of computationally designed PSs. With a change in the spin system and dipolar couplings of interest, the temperature and scoring parameters needed to be re-tuned for optimal performance. Furthermore, while the choice of 6 subdwells was proven to be sufficient for evolving $^{1}\text{H}^{-15}\text{N}$ DC's, there was no prior assurance that it would be appropriate for $^{13}\text{C}_{\alpha}^{-1}\text{H}_{\alpha}$ DC's. However, simulations have indicated that 6 subdwells with continuously applied rf power constitutes a viable choice for a generic SLF architecture, since it produces sharper and more intense dipolar peaks than PISEMA and SAMPI4 both in silica and experiment. It is also noteworthy that several ROULETTE sequences having different phases

and durations (and even power application schemes) produced NMR spectra of similar quality, which may indicate that there may be no single universal PS for such type of experiments.

8. Conclusions

We have demonstrated an improved automated design for the heteronuclear SLF sequences for measuring $^1H^{-15}N$ and $^{13}C_{\alpha}^{-1}H_{\alpha}$ DCs, which has greatly advanced the ROULETTE method. The new scoring fit function has yielded pulse sequences with consistent scaling factors and produced sharp dipolar peaks when tested experimentally. The windowless nature of the new pulse sequence makes it less susceptible to rf amplifier rise times while not requiring any 1H frequency switches as in PISEMA. Moreover, the relatively small scaling factors and short dwell times allow for measuring the much larger $^{13}C_{\alpha}^{-1}H_{\alpha}$ dipolar couplings even at moderate rf powers of 50 kHz. The presented sequences should be fully applicable at higher B_0 fields, thus benefitting from additional sensitivity and resolution.

Success in extending ROULETTE to $^{13}\text{C}_{\alpha}^{-1}\text{H}_{\alpha}$ experiments suggests that the method can be further extended for designing other oriented-sample NMR experiments involving ^{15}N , ^{13}C , and ^{1}H nuclei. With the availability of pulse sequences involving ^{13}C dimensions, a once elusive goal for oriented-sample NMR – determination of side-chain conformations for membrane proteins – could become attainable at last.

Declaration of Competing Interest

The authors declare that they have no known competing financial interests or personal relationships that could have appeared to influence the work reported in this paper.

Acknowledgements

This material is based upon work supported by the National Science Foundation under Grant No. MCB 1818240 and by the U. S. Army Research Office under contract number W911NF1810363.

Appendix A. Supplementary material

Supplementary data to this article can be found online at https://doi.org/10.1016/j.jmr.2020.106794.

References

[1] S.J. Opella, F.M. Marassi, J.J. Gesell, A.P. Valente, Y. Kim, M. Oblatt-Montal, M. Montal, Structures of the M2 channel-lining segments from nicotinic acetylcholine and NMDA receptors by NMR spectroscopy, Nat. Struct. Biol. 6 (1999) 374–379.

- [2] J. Wang, S. Kim, F. Kovacs, T.A. Cross, Structure of the transmembrane region of the M2 protein H+ channel, Prot. Sci. 10 (2001) 2241–2250.
- [3] F.M. Marassi, S.J. Opella, Simultaneous assignment and structure determination of a membrane protein from NMR orientational restraints, Prot. Sci. 12 (2003) 403–411.
- [4] N.J. Traaseth, J.J. Buffy, J. Zamoon, G. Veglia, Structural dynamics and topology of phospholamban in oriented lipid bilayers using multidimensional solidstate NMR, Biochemistry 45 (2006) 13827–13834.
- [5] N.J. Traaseth, K.N. Ha, R. Verardi, L. Shi, J.J. Buffy, L.R. Masterson, G. Veglia, Structural and dynamic basis of phospholamban and sarcolipin inhibition of Ca2+-ATPaset, Biochemistry 47 (2008) 3–13.
- [6] R. Verardi, L. Shi, N.J. Traaseth, N. Walsh, G. Veglia, Structural topology of phospholamban pentamer in lipid bilayers by a hybrid solution and solid-state NMR method, Proc Natl Acad Sci U S A 108 (2011) 9101–9106.
- [7] K. Yamamoto, M. Gildenberg, S. Ahuja, S.C. Im, P. Pearcy, L. Waskell, A. Ramamoorthy, Probing the Transmembrane Structure and Topology of Microsomal Cytochrome-P450 by Solid-State NMR on Temperature-Resistant Bicelles, Scientific Reports 3 (2013) 2556.
- [8] M. Sharma, M.G. Yi, H. Dong, H.J. Qin, E. Peterson, D.D. Busath, H.X. Zhou, T.A. Cross, Insight into the Mechanism of the Influenza A Proton Channel from a Structure in a Lipid Bilayer, Science 330 (2010) 509–512.
- [9] A. Gayen, J.R. Banigan, N.J. Traaseth, Ligand-Induced Conformational Changes of the Multidrug Resistance Transporter EmrE Probed by Oriented Solid-State NMR Spectroscopy, Angew Chem Int Edit 52 (2013) 10321–10324.
- [10] M.K. Reddy, E. Varathan, N.P. Lobo, A. Roy, T. Narasimhaswamy, K.V. Ramanathan, Mono layer to Interdigitated Partial Bilayer Smectic C Transition in Thiophene-Based Spacer Mesogens: X-ray Diffraction and C-13 Nuclear Magnetic Resonance Studies, Langmuir 31 (2015) 10831–10842.
- [11] A.A. Boopathi, K. Janani, N.P. Lobo, T. Narasimhaswamy, C-13 NMR Investigations of Hairy-Rod-Like pi-Conjugated Mesogens, Journal of Physical Chemistry B 123 (2019) 5651–5664.
- [12] J. Lapin, A.A. Nevzorov, Validation of protein backbone structures calculated from NMR angular restraints using Rosetta, Journal of Biomolecular Nmr 73 (2019) 229–244.
- [13] E.O. Awosanya, J. Lapin, A. Nevzorov, NMR" Crystallography" for Uniformly (13C, 15N) Labeled Oriented Membrane Proteins, Angew Chem Int Ed Engl (2019)
- [14] C.H. Wu, A. Ramamoorthy, S.J. Opella, High-resolution heteronuclear dipolar solid-state NMR spectroscopy, J. Magn. Reson. A 109 (1994) 270–272.
- [15] S.V. Dvinskikh, K. Yamamoto, A. Ramamoorthy, Heteronuclear isotopic mixing separted local field NMR spectroscopy, J. Chem. Phys. 125 (2006) 034507.
- [16] A.A. Nevzorov, S.J. Opella, Selective averaging for high-resolution solid-state NMR spectroscopy of aligned samples, J. Magn. Reson. 185 (2007) 59-70.
- [17] M. Veshtort, R.G. Griffin, SPINEVOLUTION: a powerful tool for the simulation of solid and liquid state NMR experiments, Journal of Magnetic Resonance 178 (2006) 248–282.
- [18] H.J. Hogben, M. Krzystyniak, G.T.P. Charnock, P.J. Hore, I. Kuprov, Spinach A software library for simulation of spin dynamics in large spin systems, Journal of Magnetic Resonance 208 (2011) 179–194.
- [19] Tošner, Z.; Andersen, R.; Stevensson, B.; Edén, M.; Nielsen, N. C.; Vosegaard, T. Computer-intensive simulation of solid-state NMR experiments using SIMPSON, J. Magn. Reson. 246 (2014) 79–93.
- [20] D. Sakellariou, A. Lesage, P. Hodgkinson, L. Emsley, Homonuclear dipolar decoupling in solid-state NMR using continuous phase modulation, Chem. Phys. Letts. 319 (2000) 253–260.
- [21] Lapin, J.; Nevzorov, A. A. De novo NMR pulse sequence design using Monte-Carlo optimization techniques, Journal of Magnetic Resonance 310 (2020), 106641.
- [22] J. Lapin, A.A. Nevzorov, Automated assignment of NMR spectra of macroscopically oriented proteins using simulated annealing, Journal of Magnetic Resonance 293 (2018) 104–114.
- [23] N. Metropolis, S. Ulam, The Monte Carlo Method, Journal of the American Statistical Association 44 (1949) 335–341.
- [24] Z. Gan, Spin dynamics of polarization inversion spin exchange at the magic angle in multiple spin systems, J. Magn. Reson. 143 (2000) 136–143.